Published in final edited form as:
Biomaterials. 2012 November ; 33(33): 8383–8394. doi:10.1016/j.biomaterials.2012.08.020.

The Regulation of Cystogenesis in a Tissue Engineered Kidney Disease System by Abnormal Matrix Interactions

B Subramanian[a,b], **W Ko**[a], **V Yadav**[a], **T DesRochers**[a], **R Perrone**[c], **J Zhou**[d], and **D Kaplan**[a,*]

[a]Department of Biomedical Engineering, Tufts University, Medford, MA 02155, USA

[b]Biomedical Engineering and Biotechnology Program, University of Massachusetts Lowell, Lowell, MA 01854, USA

[c]Division of Nephrology, Tufts Medical Center, Tufts University School of Medicine, Boston, MA 02111, USA

[d]Renal Division, Brigham and Women's Hospital, Harvard Medical School, Boston, MA 02115, USA

Abstract

Autosomal Dominant Polycystic Kidney Disease (ADPKD) remains a major health care concern affecting several million patients worldwide and for which there is no specific treatment. We have employed a 3D tissue engineered disease-like system to emulate cystic structures *in vitro* and analyzed the extracellular matrix (ECM) interactions in it. The tissue system was developed by culturing normal or polycystin-1 silenced mouse Inner Medullary Collecting Duct (mIMCD) cells in ECM infused into 3D porous silk protein biomaterial scaffolds. In this system, the silk scaffolds provide slow degradation, biocompatibility, and maintain structure and transport for the 3D system, while the ECM molecules retain biological signaling. Using this 3D tissue system we provide evidence for an autocrine signaling loop involving abnormal matrix deposition (collagen type IV and laminin) and its integrin receptor subunit protein (Integrin-β1) in *Pkd1* silenced mIMCD cells. In addition, we report that abnormal pericystic ECM interactions between matrix molecules and integrin subunit proteins regulate the rate of cystogenesis in the disease system. Molecular signaling showed abnormalities in cyclin proteins and cell-cycle progression upon *Pkd1* knockdown. Importantly, disruption of the abnormal matrix interactions by an additional knockdown (double-silencing) of integrin-β1 in *Pkd1* silenced cells reversed the abnormalities and reduced the rate of cystogenesis. Together, these findings indicate that abnormal matrix deposition and altered integrin profile distribution as observed in ADPKD and are critical in cystogenesis and should be considered a target for the development of therapeutics.

1. Introduction

Cystic Kidney Disease is a heterogeneous disease group characterized by fluid filled epithelial-lined cyst formation from renal tubules [1]. Autosomal Dominant Polycystic Kidney Disease (ADPKD) is the most common subtype, causing bilateral kidney

*Corresponding author. Prof. David Kaplan, Chair, Department of Biomedical Engineering, 4 Colby Street, Medford, MA 02155. Tel: +1-617-627-3251, Fax: +1-617-627-323, david.kaplan@tufts.edu.

enlargement due to progressive cyst formation [1–3]. Alterations in the genes *PKD1* (Polycystin-1) and/or *PKD2* (Polycystin-2) initiate cyst formation with manifestations in abnormal proliferation, differentiation and apoptosis [3]. Mutations in *PKD1* are associated with 85% of patients, while mutations in *PKD2* are associated with ~10% of patients [3]. Polycystin-1 is a large membrane spanning protein that is implicated in cell-cell and cell-extracellular matrix (ECM) interactions [4]. Polycystin-1 can also interact with Polycystin-2, which functions as a non-selective cation channel, and acts as a mechanosensor in cilia [5,6]. Current research suggests that ciliary signaling defects trigger cyst formation and progression, along with other pericystic ECM anomalies [3]. Aberrations in several intracellular signaling pathways, such as Janus Kinase/Signal Transducer and Activator of Transcription (JAK/STAT), mammalian target of Rapamycin (mTOR), Planar cell polarity (PCP) and cystic fibrosis trans membrane conductance regulator protein (CFTR) have been observed and implicated in cyst progression [7–11]. However, the precise events involved in cyst formation and progression remain largely unknown.

To date, animal models have been widely used for the understanding of polycystin function and the molecular mechanisms of cystogenesis [12]. Although they were informative, the complexity of *in vivo* models and the interference of evolving mechanisms of post gene alterations have left the cyst-driving events elusive. In contrast, 3D *in vitro* systems provide the ease of system- manipulation, the ability to track changes over relatively short timeframes, and the low cost compared to mice. Current 3D *in vitro* gel cultures lack structural support for the tissue systems and develop excessive contraction that alters the matrix-biophysical properties that regulate epithelial morphogenesis [13]. Tissue engineering strategies originally developed for the restoration of organ functions have been suggested as an alternate option for the development of relevant tissue systems for research needs. Tissue engineering strategies for kidney have been used to restore functions in animal models either by mimicking the developmental stages in the kidney or by providing a predefined kidney structure-based system [14]. Despite these advances in kidney tissue engineering, the development of 3D kidney-tissue models remains minimal. To address this issue, we have previously developed a hybrid kidney tissue system encompassing the ECM to simulate the developmental stages and an engineered silk-based 3D scaffold to provide structural support for the system [15]. We have also demonstrated the sustainability of these tissues for longer time periods by perfusion in a bioreactor [15]. In this study we have used the system to investigate the molecular signaling associated with cyst formation.

The objective of the present study was to investigate the significance of matrix interactions in ADPKD using a 3D engineered tissue system. Our hypothesis was that loss of PKD1 function would result in altered matrix interactions leading to cystogenesis as seen in ADPKD. The outcome from this study would provide insights into the molecular mechanisms delineating the significance of abnormal matrix interactions in cystogenesis and in the long run would contribute to the development of therapeutics for ADPKD.

2. Materials and Methods

2.1. Cell Culture

Mouse Inner Medullary Collecting Duct cells (mIMCD cells) (CRL-2123, ATCC, Manassas, VA) were maintained in Dulbecco's Modified Eagle Medium: Nutrient Mixture F-12 (DMEM/F12) (Invitrogen, Carlsbad, CA) supplemented with 10% fetal bovine serum (Invitrogen, Carlsbad, CA) and 1% penstrep (Invitrogen, Carlsbad, CA).

2.2. RNAi

shRNA sequences targeting *Pkd1* were cloned into LentiLox plasmid (pLL3.7) (Addgene, Cambridge, MA). Lentivirus particles were produced by a transient transfection of lentivector plasmid and other packaging plasmids in 293FT cells (Invitrogen, Carlsbad, CA). Virus particles were quantified by p24 ELISA (Zeptometrix, Buffalo, NY) and Multiplicity of Infection (MOI) was calculated. mIMCD cells were infected at <50% confluency for 24 h at MOI 10 and transduction efficiency was determined based on green fluorescence protein (GFP) in flow cytometry at 48 h post infection. Transduced cells were sorted and established as a polyclonal cell population. For double-silencing the gene encoding integrin-β1 (*Itgb1*), viral particles derived from pLKO vector with validated shRNA sequences were used (Sigma-Aldrich, St. Louis, MO). Transduced cells were selected with 10 μg/mL puromycin.

2.3. Proliferation Assay

Proliferation rate of the cells were measured by Alamar Blue assay (Invitrogen, Carlsbad, CA). Briefly, equal numbers of cells were plated in 2% reduced serum followed by incubation in a media with Alamar dye for 3 h. Sample aliquots were collected and fluorescence was measured. Cells were then switched to dye free media for further proliferation and the procedure was repeated at the next time point of analysis. Samples collected from 6 h post plating were used as 0 h reading in the analysis. Subsequent measurements were made at 24 hour intervals post 0h reading. All sample aliquots were collected at semiconfluent culture condition and the experiment was ended if any of the groups reached ~75% confluence. Three independent experiments were done in triplicates.

2.4. 3D Tissue Engineered Culture Systems

Aqueous silk scaffolds were prepared from silk fibroin solution extracted from *Bombyx mori* as we have described previously [15]. The final dimensions of the scaffolds were 6 mm × 2 mm (diameter × height). Tissue engineered constructs were developed by mixing cells with a 1:1 (vol/vol) mix of collagen type I (1 mg/mL and Matrigel™ (BD Biosciences, Rockville, MD) to a final concentration of 2×10^6 cells/mL and then added to the scaffolds. The pores of the scaffolds were filled with the cell-matrix mix and allowed to gel for 30 minutes at 37°C. Cells were maintained in static culture conditions and media was changed-by-half on alternate days.

2.5. Transport Assay

Scaffolds were incubated in phenol red free plain DMEM/F-12 media for 12 h, followed by addition of Rhodamine (Sigma, St.Louis, MO) for 12 h. Following uptake, scaffolds were washed with PBS three times and imaged as whole scaffold live cell imaging in confocal microscopy. Total numbers of structures included for analysis and their percent positive for rhodamine uptake are provided. Three independent experiments were done in triplicates and similar counts were used for analysis. Counts from one experiment (n – value) and the percentage of the rhodamine positive cysts with representative images were included.

2.6. Immunoblotting

Cells were lysed in a Radio Immuno-precipitation Assay (RIPA) lysis buffer (Pierce Biotechnology, Rockford, IL) with Halt™ protease and phosphatase inhibitors (Pierce Biotechnology, Rockford, IL) and the total cell proteins were collected by centrifugation at 14,000 g for 15 minutes. Equal amounts of protein samples were electrophoresed in 4–12% Bis-Tris gel (Invitrogen, Carlsbad, CA) and transferred to a poly-vinylidenefluoride (PVDF) membrane (Invitrogen, Carlsbad, CA). Probing with primary antibodies for Pkd1 (sc130554-1:1000), Integrin-β1 (sc8978-1:1000) (Santa Cruz Biotechnology Inc, Santa Cruz, CA) and with antibodies for laminin (ab11575-1:2000), collagen-IV (ab6586-1:2000)

and cyclinD1(ab16663-1:200) (Abcam Inc, Cambridge MA) were performed in 3% skimmed milk, whereas glyceraldehyde-3-phosphate dehydrogenase (GAPDH) (ab9484-1:2000) and cyclinE (ab2959-1:2000) (Abcam Inc, Cambridge MA) were probed in 5% bovine serum albumin (BSA). Secondary antibodies conjugated with horse radish peroxidase (HRP), (Goat Anti-rabbit HRP – sc2004 or Goat Anti-mouse HRP – sc2005) (Santacruz Biotechnology, Santacruz, CA) were used according to the primary antibody host. Pkd1 blotting was developed using ECL Advance reagents while other proteins were developed using ECL plus reagents (GE Healthcare Biosciences, Piscataway, NJ).

2.7. Cell Cycle Analysis

Cells were trypsinized and collected at specific time intervals. Cells were fixed in 70% ice-cold ethanol and stored at −20°C overnight. Cells were then washed in PBS and re-suspended in a DNA staining solution (2.5 μg /mL propidium iodide and 1 mg/mL RNase A in PBS) for 1h at 4°C. Samples were run in a flow cytometer system (FACS Calibur, BD Biosciences, CA) and the results were analyzed using Flow Jo software (Treestar, Ashland, OR). Three independent experiments were performed in triplicate.

2.8. Histology and Fluorescence Imaging

Formalin fixed 5 μm scaffold sections were deparraffinized and stained for Hematoxylin and Eosin (H&E) as described previously [15]. For immunofluorescence, 5 μm sections were deparaffinized and antigen retrieval was performed with Antigen Unmasking Solution (Vector Laboratories, Burlingame, CA) by boiling slides for 30 minutes. After antigen retrieval, scaffold sections were blocked with 5% bovine serum albumin (BSA) supplemented with 10% serum from the secondary antibody host, in Dulbecco's Phosphate Buffered Saline (DPBS) (Invitrogen, Carlsbad, CA). E-cadherin was probed with rabbit polyclonal IgG (ab53033-1:50) (Abcam, Cambridge, MA) and goat polyclonal to rabbit IgG-Cy5 conjugate (ab6564-1:75) (Abcam, Cambridge, MA). N-cadherin was probed with mouse monoclonal IgG (ab66025-1:50) (Abcam, Cambridge, MA) and goat polyclonal to mouse IgG-FITC conjugate (ab6785-1:75) (Abcam, Cambridge, MA). For collagen-IV (1:40), laminin (1:50) and cyclin-D1 (1:20), primary antibodies described in the immunoblot section were used, while for integrin –β1, rabbit IgG (ab52971-1:25) (Abcam, Cambridge, MA) was used. Goat polyclonal to rabbit IgG-Cy5 conjugate (ab6564-1:75) (Abcam, Cambridge, MA) was used as the secondary antibody for these proteins. Similarly for acetylated alpha-tubulin, anti-sera from clone (6-11B-1) (T6793-1:25) (Sigma-Aldrich, St.Louis, MO) and goat polyclonal mouse IgG-Cy5 (ab6563-1:50) (Abcam, Cambridge, MA) were used. Slides were counterstained for the nucleus using 4, 6- Diamidino-2-phenylindole (DAPI) (Invitrogen, Carlsbad, CA) and mounted with Fluoroguard antifade reagent (Bio-Rad, CA).

2.9. Confocal Microscopy and Image Analyses

Cells were viewed with an Ar/Kr laser (488 nm) or He/Ne laser (633 nm) in conjunction with a confocal laser scan head in a Leica TCS SP2 Microscope. Digital images were collected with a 20× lens coupled with ~7X digital zoom. For quantification of cyst size, images were collected in transmission mode and the size of the cysts was measured by evaluating the length of the longest axis observed in the cystic-structures. For relative quantification of protein expression in cysts, images were collected with similar Photomultiplier tube (PMT), pinhole and offset settings for normal and disease tissue samples. Total number of structures included for analysis and their percent positive for protein/dye staining are provided. For fluorescence intensity quantification, Region Of Interest (ROI) encompassing the cystic structures were defined using the quantification tools in the Leica Confocal Suite and the fluorescence intensity per area units were calculated. The quantification procedure for a representative image is given in Supplementary Figure 1.

2.10. mRNA expression analysis

Total RNA was extracted using an RNAeasy Mini Kit (Qiagen, Santa Clarita, CA) and quantified by UV absorbance at 260 nm. Four micrograms of RNA was reverse transcribed into cDNA using a high capacity cDNA archive kit (ABI Biosystems, Foster City, CA). Polycystin-1 expression levels were then determined using a QuantiTect SYBR green kit (Qiagen, Santa Clarita, CA) using primers 5' TATCTGCAGTACCGACTGTGTTACC 3' and 5' TTGAACTGGCGGAGTACCTG 3' and normalized with GAPDH expression levels.

2.11. Graphical and Statistical Analyses

Statistical analyses were carried out using GraphPad Instat software (GraphPad Inc., La Jolla, CA). Data were analyzed using one-way analysis of variance (ANOVA) and when statistical significance was seen by ANOVA, the Student–Newman-Keuls separation of means was used to find group differences. Statistical significance was set at minimal value of $p<0.05$ and all values are expressed as mean ± standard deviation. Graphical representations of data were generated in GraphPad Prism 5 software (GraphPad Inc., La Jolla, CA).

3. Results

3.1. Generation and Characterization of Stable Pkd1 Silenced Cell Lines

Lentiviral vectors were used to post-transcriptionally silence *Pkd1* in mIMCD cells. shRNA sequences for *Pkd1* with their targeting sites are provided in Supplementary Figure 2A. These vectors also carry a GFP reporter gene, which was used to evaluate the transduction efficiency and for sorting the cells. The transduction efficiency at 48 h post infection was ~25% for shRNA vectors (*Pkd1* silenced) and ~30% for empty vectors (Control) (Figure 1A). Cells were then sorted for GFP and cultured for more time to attain sufficient cell populations for evaluating *Pkd1* silencing by immunoblotting. Cells transduced with empty vector showed similar Pkd1 expression levels as normal cells, whereas cells transduced with shRNA sequences had varying levels of reduction (Supplementary Figure 2B). Cells with the greatest reduction of polycystin-1 (~85% reduction) were designated as *Pkd1* silenced and used in subsequent experiments (Figure 1B and Supplementary Figure 2B) to mimic the loss of gene function phenotype. As there are not many good antibodies to detect polycystin-1 protein, we have also confirmed the Pkd1 knockdown in these cells using RT-PCR. The results indicated ~70% reduction in *Pkd1* silenced cells (Figure 1C), unlike in the control cells.

Loss of polycystin-1 function has been shown to cause hyper-proliferation, whereas overexpression of polycystin-1 has been shown to inhibit cell growth [16–19]. We characterized the cells by evaluating the proliferation of *Pkd1* silenced cells. The results indicated that *Pkd1* silenced cells proliferated at a significantly higher rate than the normal and empty vector transduced cells (Figure 1D). In addition, the proliferation data indicated that control cells proliferated at a similar rate as normal cells. Therefore, based on the similar protein levels and proliferation data, we used control cells (empty vector transduced) to mimic normal tissue and the *Pkd1* silenced cells to mimic diseased tissue in all of the following experiments, unless otherwise specified.

3.2. Cystic Kidney Tissue Model

Tissue engineering strategies for the kidney have allowed the development of constructs for restoring the kidney functions [14]. However, none of these systems recapitulate the *in vivo* like 3D microenvironment similar to cystic kidneys and to investigate the dynamic changes associated with cyst formation and expansion. Previously, we developed a strategy of employing silk scaffolds and natural ECM molecules to develop a long-term 3D *in vitro* co-

cultured kidney tissue model [15]. Here we have utilized a similar strategy, but limited to a single cell type, mIMCD cells, and shorter time frames for developing 3D models of normal-like and ADPKD disease-like tissue (Figure 2A). Our results indicate that both control and *Pkd1* silenced cells were able to undergo morphogenesis and form organized structures (Figure 2B). However, cystic tissues from ADPKD are known to manifest abnormalities both in structure and function. Therefore we assessed the quality of our tissues both in terms of structure and function. We assessed the structure using cell junction marker proteins such as E-cadherin and N-cadherin, as abnormalities in their patterns were observed in ADPKD tissues [20, 21]. The results showed cell-cell adhesion site distribution for E-cadherin in both normal and disease tissue (n=69, 92% stained positive) (Figure 2C). Whereas, the cell-cell adhesion site distribution pattern for N-cadherin (n=62, 87% stained positive) was observed only in the disease-like tissue but not for normal-like tissue (Figure 2C). These results were in accordance with the literature, i.e. abnormal N-cadherin expression is detected in ADPKD but not in normal adult kidney tubules [20]. Though we observed neo-expression of N-cadherin, we also observed mis-localized E-cadherin in the cystic structures. Previous evidence has shown that polycystin-1 interacts with E-cadherin and play a role in early stages of cell-cell junction assembly [20, 22]. However, it is unclear at what stages the complete loss of E-cadherin is observed in cyst progression. In addition, gene regulatory mechanisms relating E-cadherin and polycystin-1 levels are not known. We speculate that the mis-localization of E-cadherin and neo-expression of N-cadherin could be associated with early stages of cyst progression, and as the cyst enlarges, a more dedifferentiated phenotype could be manifested leading to the complete loss of E-cadherin expression. This may be the reason for some overlapping E-cadherin and N-cadherin expression in some of the cystic structures in the kidney [20] and in our present system. Furthermore, ADPKD tissues exhibit abnormal transport properties [23], thus we assessed transport function. Organic anion transport, which is known to be minimal in the collecting duct cells of the nephron [24], was assessed. As shown in Figure 2D, the disease tissue showed increased transport of rhodamine into the luminal space (n=50, 98% stained positive) while the normal tissue had minimal uptake of rhodamine into cells (n=57, 91% stained positive), suggesting an abnormality in transport properties in the disease tissue. These results indicate that the engineered constructs were exhibiting features of both normal and disease conditions and provide an alternate yet relevant system for conducting systemic analysis in ADPKD.

3.3. Loss of Pkd1 Causes Abnormal Matrix Interactions in Cystogenesis

ADPKD is known to develop several structural aberrations including changes in basement membrane composition and cell-ECM interactions [25–28]. However, the source of excessive pericystic ECM proteins and its significance in ADPKD remain unclear. We assessed whether the ECM abnormalities were recapitulated in our tissue system. Immunoblotting for collagen-IV and laminin proteins in total lysates showed increased expression for both, implying that the cyst-lining cells are the source of excessive matrix production in ADPKD (Figure 3A). In addition, immunostaining for collagen-IV (n=47, 88% stained positive, normal; n=51, 92% stained positive, disease) and laminin (n=69, 92% stained positive, normal; n=62, 97% stained positive, disease) in the 3D tissues showed increased expression with pericystic localization in the disease constructs (Figure 3B). Interestingly, despite the abundance of matrix proteins in the system, we observed the staining pattern only in the immediate vicinity of the cysts. This is in accordance with other reports suggesting that ECM proteins assembled on the surface of tissue structures alone would be detected by immunofluorescence [29]. Furthermore, as cell-matrix interactions are mainly mediated through integrins, we assessed the significance of excessive matrix production by evaluating integrins known to be associated with collagen type IV and laminin. In particular, we analyzed the integrin-β1 subunit expression as they are primarily

known to mediate the ECM signaling and also known to be aberrant in ADPKD [26, 27]. The results indicate increased expression of integrin-β1 in total lysates and 3D constructs (n=82, 87% stained positive, normal; n=78, 91% stained positive, disease) (Figure 3A and B).

These results suggested that the loss of Pkd1 function leads to an autocrine signaling loop as evident from excessive basement membrane matrix protein deposition and production of its known receptor subunit, integrin-β1. In addition to the matrix interactions, as ciliary signaling defects are also associated with cystogenesis [30], we assessed whether or not our tissue systems were exhibiting ciliary structures. Immunostaining showed the presence of cilia in both the normal and disease tissues and the results were quantified as positive for cilia per cyst (n=42, 89% of the cystic structure sections stained positive, normal; d=57, 97% of the cystic structure sections stained positive, disease) (Figure 3C). Although these data support the utilization of the system for ciliary signaling analysis, in this study we have limited our focus to analyzing abnormal matrix signaling in cystogenesis. However, the system could also be used to evaluate ciliary signaling in cystogenesis and probe for changes in length and function as described previously [31].

3.4. Abnormal Matrix Interaction Caused an Increased Rate of Cystogenesis

Routine 3D culture of normal and *Pkd1* silenced cells in our tissue engineered systems showed larger cyst formation in the disease tissue. Although this could be attributed to the increased proliferation rate of *Pkd1* silenced cells (Figure 1D), the underlying signaling mechanisms and their effects, in particular, in 3D systems are unknown. ECM composition and interactions have been primarily known to regulate the morphogenetic behavior of cells in 3D culture [32]. As our tissue model recapitulates the abnormalities of pericystic ECM and its interacting protein – integrin-β1, we also checked if a similar trend of increased integrin-β1 and matrix proteins is observed in *in vivo* tissues. Our results on $Pkd1^{-/-}$ knockout mouse kidneys (Jing Zhou, BWH) [33] confirmed the increased expression pattern of these proteins in cystic kidneys (Figure 3D). Given these evidence, we hypothesized that the abnormal matrix interactions cause larger cyst formation. We evaluated the effect of abnormal matrix interactions in our 3D tissue systems by double silencing the gene encoding integrin-β1 (*Itgb1*) in *Pkd1* silenced cells. The development and designation of symbols for double infected cells are shown in Figure 4A. Immunodetection of integrin-β1 shows (>90%) reduction in *Itgb1* silenced cells and (~80%) in *Pkd1* & *Itgb1* silenced cells (Figure 4B). Furthermore, our results in 3D culture systems showed a difference in cyst size as shown in the Figure 4C. Quantification of the cystogenesis rate in these cells showed an increased rate of cystogenesis resulting in larger cysts in *Pkd1* silenced^2 cells and this was reversed to normal conditions in *Pkd1* & *Itgb1* silenced cells (Figure 4D). This is also evident from the representative histological sections collected at different time points (Figure 4E). In addition, cyst size quantification values with lower error bars indicated minimal structural heterogeneity within the respective groups in the system (Figure 4D). Altogether, these results indicated that the rate of cystogenesis was regulated by abnormal matrix interactions and could be reduced by silencing *Itgb1.*

3.5. Abnormal Matrix Interactions are Associated with Altered Proliferation and Cell Cycle Changes

Cell cycle changes have been implicated in cyst derived cells for increased proliferation and cyst progression [34, 35]. We tested whether the aberrant rate of cystogenesis was due to changes in proliferation and cell cycle. Cell proliferation assays showed an increased rate in *Pkd1* silenced^2 cells that was restored to normal conditions in *Pkd1* & *Itgb1* silenced cells (Figure 5A). To further understand this response, we evaluated the fluctuation of the cell cycle protein, Cyclin-D1, over a time profile of 0–25 h after serum starvation. We observed

a constitutively increased Cyclin-D1 pattern in *Pkd1* silenced^2 cells and the restoration to normal conditions in *Pkd1* & *Itgb1* silenced cells (Figure 5B). Similarly, Cyclin-E collected at similar conditions showed maximum elevation earlier (5h) in *Pkd1* silenced^2 cells and restoration to normal (10 h) in *Pkd1* & *Itgb1* silenced cells (Figure 5B). Furthermore, cell cycle analysis showed an earlier increase in cell number in S –Phase for *Pkd1* silenced^2 cells, but similar to control^2 cells in *Pkd1* & *Itgb1* silenced cells (Figure 5C and Supplementary Figure 3). In addition, we did not see any significant change in *Itgb1* silenced cells. These results indicated that increased protein in *Pkd1* silenced cells was associated with an accelerated G1-S phase entry in the cells and could be reversed by reducing the integrin-β1 proteins. To determine whether this is also true in 3D we immunostained day-7 cysts for cyclin-D1. In accordance with the cyclin-D1 pattern, we observed an increase in cyclin-D1 in the disease cystic tissue and a reduction in *Pkd1* & *Itgb1* silenced cystic tissues (Figure 6A).

Altogether, we demonstrated that tissue engineering strategies provide ways to develop relevant kidney tissue models with features similar to *in vivo* conditions. In addition, our results have shown that abnormal matrix interactions in ADPKD regulate the rate of cystogenesis that are mediated by aberrant proliferation and cell cycle changes, resulting in larger cyst formation in *Pkd1* silenced cells (Figure 6B).

4. Discussion

To evaluate the significance of abnormal ECM interactions in ADPKD, we employed our previously established 3D *in vitro* culture system, utilizing scaffold-based tissue engineering to mimic normal-like and disease-like conditions of ADPKD [15]. Although, other 3D gel systems could be used to investigate mechanisms of cystogensis, gel contraction can impact or modulate the morphogenetic behavior of the cells [13] and could lead to a mix of cysts and branching structures. For the needs of the study described here, a system with minimal structural heterogeneity is desired for consistent analysis. Hence, the utility of scaffolds to support the system and minimize structural variation is critical for our morphometric analysis. The use of silk protein porous scaffolds provides the advantage of preventing contraction over time [15], and supports subsequent biochemical and morphometric analysis. Silk-biomaterials were selected as scaffold biomaterial due to the wide range of relevant properties; for example, the presence of diverse amino acid side chains to facilitate coupling chemistry to functionalize the materials; versatile processing into hydrogels, ultrathin films and porous matrices for broad utility [36–38]. Here we have used aqueous-derived porous silk scaffolds to support cystic structures in the pores of the scaffolds. In addition, we have used our system as shorter time frame static cultures as typically seen in other 3D gel systems, to allow us to relate our outcomes with other prior studies of ADPKD over similar time frames. Overall, the silk scaffold approach is also useful for sustaining tissues for longer time frames [15] and also for molecular signaling analysis without morphogenetic heterogeneity as shown here.

Numerous studies have shown structural and functional abnormalities in ADPKD kidneys. In this study, we utilized lentivirus-mediated *Pkd1* silencing in a well-characterized cell line, mIMCD, to induce a pathognomonic state similar to ADPKD. Silencing of *Pkd1* reduced the functional polycystin-1 and resulted in a haploinsufficient condition that could induce cyst formation as observed in hypomorphic *Pkd1*^{nl} models [39]. In accordance, we demonstrated that *Pkd1* silenced cells induced abnormal cyst formation and altered structure and function in terms of marker protein expression (E-cadherin and N-cadherin) and organic anion transport (Figure 2). Our system provided an alternate, yet relevant platform to study the pathology in a haploinsufficient condition, inducing cystic structures with features similar to the cystic kidneys of ADPKD.

Constitutive ECM microenvironment remodeling is essential in facilitating cyst progression in ADPKD. Previous studies have shown a critical role for integrins, in particular integrin-β1, in mediating ECM signaling and kidney branching morphogenesis [40, 41]. In addition, co-localization of integrin-β1 with laminin-5 is observed in cyst-derived cells and is implicated in mediating the effects of basement membrane changes [28]. Though these abnormal matrix interactions are observed in several animal models of ADPKD and in human patient samples, their significance in ADPKD pathology is poorly understood. We have started to analyze the significance of this ECM deposition in ADPKD cystogenesis. We have used the polycystin-1 silenced cells to investigate the significance of ECM interactions, in particular integrin-β1 mediated ECM interactions, in cystogenesis. Here, we have shown that loss of polycystin-1 induces a constitutive autocrine loop in which cells deposit their own aberrant ECM proteins (Collagen IV and Laminin) and also up-regulate its receptor proteins (Integrin-β1) to promote cell proliferation and cyst progression (Figure 3), which is in agreement with the expression pattern observed in autosomal dominant polycystic kidney disease [42]. Although, we observed an increased expression for integrin-β1 in our disease tissue system, they exhibited both apical and baso-lateral distribution, while the normal cells exhibited baso-lateral distribution. Earlier evidence at least from *Pkd1*$^{-/-}$ kidneys has shown that increased distribution is localized to both membrane and cytoplasmic regions [43]. Although speculative, our consistent observation of integrin-β1 limited to membrane distribution suggests that evolving mechanisms would have facilitated a cytoplasmic localization in *Pkd1*$^{-/-}$ kidneys. Furthermore, this contrasting phenotype of both membrane and cytoplasmic distribution of integrin-β1 in *Pkd1*$^{-/-}$ kidney sections is attributed to the Golgi-complex and membrane localization for α3β1 integrins [43]. However, it is unclear, whether the apical distribution indicates for any loss of polarity, as both polycystin-1 and integrin-β1 are associated with apico-basal polarity pathways [44, 45]. In addition, recent data suggest a possible involvement of integrin-β1 in Planar Cell Polarity signaling [46], which is also implicated in cyst formation [9]. These data clearly indicate that the relations between polycystin-1, ECM - intergin interactions, and cystogenesis are complex with numerous cross connections with other pathways. Nevertheless, with a simple *in vitro* culture system this work clearly indicates that the loss of Pkd1 triggers changes in the cell micro-environment with abnormal ECM (Collagen IV and laminin) and integrin-β1, and might be associated with the initiating events in cyst formation, which is in accordance with observations in the basement membrane of the earliest detectable cysts [25].

A role for integrin-β1 in *Pkd1* silenced cells was initially recognized through α2β1 integrins in anoikis resistance in MDCK cells [18]. Though, integrin-β1 up-regulation is observed in *Pkd1* silenced cells, recent evidence have also shown that loss of integrin-β1 in earlier stages of gestation could also form dilated tubules. The reasons for these apparent opposite observations are yet unknown. Possibly, as polycystin-1 is known to co-immunopercipitate with integrin-β1 [47] delicate balance of these protein levels in developmental stages might be critical to regulate kidney tubule structure. In accordance with this, disruption of polycystin-1 function in renal developmental stages is also known to define the rate of cyst formation in kidneys. *Pkd1* inactivation before postnatal day 13 results in severe cystic kidneys, while after day 14 or in adulthood results in fewer cysts [48, 49]. However, the significance of polycystin-1 signaling in the context of matrix interactions and ADPKD cystogenesis is not known. Given that our *Pkd1* silencing is constitutive with recapitulation of epithelial tissue morphogenesis, our system would provide a platform to investigate the signaling mechanisms associated with accelerated cyst formation as observed in developing kidneys. This is evident from our observation of an increased rate of cystogenesis in disease tissue. Earlier reports have shown abnormal proliferation and involvement of several signaling pathways such as mTOR and JAK/STAT in ADPKD cyst formation [7–11]. Though these signaling mechanisms are significant in cyst development, the ECM-mediated tissue morphogenesis resulting in multicellular organized tissue structures suggests that

there exists abnormal matrix mediated signaling, which drives subsequent intracellular signaling changes and progressive cyst formation. Our findings indicate that the increased rate of cystogenesis is associated with an autocrine loop of ECM and integrin-β1 interactions and could be restored to normal conditions by reducing integrin-β1 levels (Figure 3&4). Surprisingly, we have not seen any significant changes in the integrin-β1 silenced cells in our system. Previous data from MDCK cells based collagen gel cultures have shown that disruption of the integrin-β1 interaction with a blocking antibody results in disorganized cystic structures and could be recovered with endogenous laminin [44]. This led us to speculate that the presence of exogeneous laminin molecules in the matrix could have contributed through similar pathways for the morphogenesis of these cells.

As previously mentioned integrin-β1 is known to provide resistance to anoikis through α2β1 integrins in *Pkd1* silenced MDCK cells [18]. This finding is intriguing, as there could be potential involvement of apoptosis resistance in the alteration of cystogenesis kinetics. However, our results on apoptosis, based on Annexin V staining in serum starved cells, showed minimal differences in apoptosis sensitivity between control and *Pkd1* silenced cells (Supplementary Figure 4), suggestive of processes different from apoptosis that alter the rate of cystogenesis. In addition, larger cyst sizes could be due to cyst dilation. However, the observation of more nuclei in larger cyst structures in *Pkd1* silenced cells suggested for a possible role for defects in proliferative mechanisms in determining cyst size. Hence, our proposed mechanism for the increased rate of cystogenesis, that abnormal autocrine signaling involving matrix interactions, leads us to believe that the dysregulation of proliferative mechanisms is associated with the increased rate of cystogenesis. We have shown that the increased proliferation in *Pkd1* silenced cells could be reversed effectively by interfering with the abnormal matrix interactions through double silencing *Itgb1*. Other reports have also shown a direct link for relating polycystins with the proliferation by regulating the cell cycle [50]. We investigated whether or not the changes observed in *Pkd1* silenced[2] cells were due to proliferation and cell cycle changes that are also associated with abnormal matrix interactions. Our cell cycle analysis studies showed an accelerated S-phase entry triggered in *Pkd1* silenced cells[2] by constitutive cyclin-D1 expression and reversed in *Pkd1* & *Itgb1* silenced cells. In accordance, elevation of cyclin-D1 in our 3D system is also observed for disease tissue. However, it is not known whether the increased cyclin-D1 expression is due to an inhibition in degradation or increased expression of protein. In addition, we were also unable to find nucleus positive cyclin-D1 cells in our system, suggesting for future studies focused on the cyclin-D1 localization and expression regulation and its consequences in the cystogenesis process.

5. Conclusions

We have developed a silk scaffold and natural ECM based cystogenesis system for normal-like and disease-like tissues, and identified that loss of polycystin-1 function leads to an induction of an autocrine loop signaling involving abnormal ECM protein deposition and expression of its related integrin receptor protein, as shown in 3D engineered culture systems for disease-like tissues. In addition to their association with the increased rate of cystogenesis in the disease-like tissues, our results delineate the underlying mechanisms associated with matrix mediated proliferation and cell cycle regulation. Together our data provide insights into the role of matrix signaling in ADPKD and thus provide new guidelines for developing therapeutics for this disease.

Supplementary Material

Refer to Web version on PubMed Central for supplementary material.

Acknowledgments

The authors thank Carmen Preda from Biomedical Engineering, Tufts University, for laboratory assistance. This research was supported by Genzyme GRIP program; Hoffmann-La Roche and the National Institute of Health Tissue Engineering Resource Center [P41 EB002520] to David Kaplan.

References

1. Bonsib SM. The classification of renal cystic diseases and other congenital malformations of the kidney and urinary tract. Arch Pathol Lab Med. 2010; 134:554–568. [PubMed: 20367308]
2. Bonsib SM. Renal cystic diseases and renal neoplasms: a mini-review. Clin J Am Soc Nephrol. 2009; 4:1998–1900. [PubMed: 19875768]
3. Igarashi P, Somlo S. Genetics and pathogenesis of polycystic kidney disease. J Am Soc Nephrol. 2002; 13:2384–2398. [PubMed: 12191984]
4. Malhas AN, Abuknesha RA, Price RG. Interaction of the leucine-rich repeats of polycystin-1 with extracellular matrix proteins: possible role in cell proliferation. J Am Soc Nephrol. 2002; 13:19–26. [PubMed: 11752017]
5. Mochizuki T, Wu G, Hayashi T, Xenophontos SL, Veldhuisen B, Saris JJ, et al. PKD2, a gene for polycystic kidney disease that encodes an integral membrane protein. Science. 1996; 31:1339–1342. [PubMed: 8650545]
6. Nauli SM, Alenghat FJ, Luo Y, Williams E, Vassilev P, Li X, et al. Polycystins 1 and 2 mediate mechanosensation in the primary cilium of kidney cells. Nat Genet. 2003; 33:129–137. [PubMed: 12514735]
7. Talbot JJ, Shillingford JM, Vasanth S, Doerr N, Mukherjee S, Kinter MT, et al. Polycystin-1 regulates STAT activity by a dual mechanism. Proc Natl Acad Sci USA. 2011; 108:7985–7990. [PubMed: 21518865]
8. Boletta A. Emerging evidence of a link between the polycystins and the mTOR pathways. Pathogenetics. 2009; 2:6. [PubMed: 19863783]
9. Luyten A, Su X, Gondela S, Chen Y, Rompani S, Takakura A, et al. Aberrant regulation of planar cell polarity in polycystic kidney disease. J Am Soc Nephrol. 2010; 21:1521–1532. [PubMed: 20705705]
10. Yang B, Sonawane ND, Zhao D, Somlo S, Verkman AS. Small-molecule CFTR inhibitors slow cyst growth in polycystic kidney disease. J Am Soc Nephrol. 2008; 19:1300–1310. [PubMed: 18385427]
11. Chapin HC, Caplan MJ. The cell biology of polycystic kidney disease. J Cell Biol. 2011; 191:701–710. [PubMed: 21079243]
12. Wilson PD. Mouse models of polycystic kidney disease. Curr Top Dev Biol. 2008; 84:311–350. [PubMed: 19186247]
13. Wozniak MA, Desai R, Solski PA, Der CJ, Keely PJ. ROCK-generated contractility regulates breast epithelial cell differentiation in response to the physical properties of a three-dimensional collagen matrix. J Cell Biol. 2003; 163:583–595. [PubMed: 14610060]
14. Perin L, Da Sacco S, De Filippo RE. Regenerative medicine of the kidney. Adv Drug Deliv Rev. 2011; 63:379–387. [PubMed: 21145933]
15. Subramanian B, Rudym D, Cannizzaro C, Perrone R, Zhou J, Kaplan DL. Tissue-engineered three-dimensional in vitro models for normal and diseased kidney. Tissue Eng Part A. 2010; 16:2821–2831. [PubMed: 20486787]
16. Nishio S, Hatano M, Nagata M, Horie S, Koike T, Tokuhisa T, et al. Pkd1 regulates immortalized proliferation of renal tubular epithelial cells through p53 induction and JNK activation. J Clin Invest. 2005; 115:910–918. [PubMed: 15761494]
17. Ramasubbu K, Gretz N, Bachmann S. Increased epithelial cell proliferation and abnormal extracellular matrix in rat polycystic kidney disease. J Am Soc Nephrol. 1998; 9:937–945. [PubMed: 9621276]

18. Battini L, Fedorova E, Macip S, Li X, Wilson PD, Gusella G. Stable knockdown of polycystin-1 confers integrin-alpha2beta1-mediated anoikis resistance. J Am Soc Nephrol. 2006; 17:3049–3058. [PubMed: 17005934]
19. Boletta A, Qian F, Onuchic LF, Bhunia AK, Phakdeekitcharoen B, Hanaoka K, et al. Polycystin-1, the gene product of PKD1, induces resistance to apoptosis and spontaneous tubulogenesis in MDCK cells. Mol Cell. 2006; 6:1267–1273. [PubMed: 11106764]
20. Roitbak T, Ward CJ, Harris PC, Bacallao R, Ness SA, Wandinger-Ness A. Polycystin-1 multiprotein complex is disrupted in polycystic kidney disease cells. Mol Biol Cell. 2004; 15:1334–1346. [PubMed: 14718571]
21. Natoli TA, Gareski TC, Dackowski WR, Smith L, Bukanov NO, Russo RJ, et al. Pkd1 and Nek8 mutations affect cell-cell adhesion and cilia in cysts formed in kidney organ cultures. Am J Physiol Renal Physiol. 2008; 294:F73–F83. [PubMed: 17928412]
22. Streets AJ, Wagner BE, Harris PC, Ward CJ, Ong AC. Homophillic and Heterophillic interactions regulate E-cadherin recruitment and junction assembly in MDCK cells. J Cell Sci. 2009; 122:1410–1417. [PubMed: 19351715]
23. Sullivan LP, Wallace DP, Grantham JJ. Epithelial transport in polycystic kidney disease. Physiol Rev. 1998; 78:1165–1169. [PubMed: 9790573]
24. Sweet DH, Eraly SA, Vaughn DA, Bush KT, Nigam SK. Organic anion and cation transporter expression and function during embryonic kidney development and in organ culture models. Kidney Int. 2006; 69:837–845. [PubMed: 16518343]
25. Cuppage FE, Huseman RA, Chapman A, Grantham JJ. Ultrastructure and function of cysts from human adult polycystic kidneys. Kidney Int. 1980; 17:372–381. [PubMed: 7401457]
26. Joly D, Morel V, Hummel A, Ruello A, Nusbaum P, Patey N, et al. Beta4 integrin and laminin 5 are aberrantly expressed in polycystic kidney disease: role in increased cell adhesion and migration. Am J Pathol. 2003; 163:1791–1700. [PubMed: 14578180]
27. Wilson PD, Burrow CR. Cystic diseases of the kidney: role of adhesion molecules in normal and abnormal tubulogenesis. Exp Nephrol. 1999; 7:114–124. [PubMed: 10213865]
28. Joly D, Berissi S, Bertrand A, Strehl L, Patey N, Knebelmann B. Laminin 5 regulates polycystic kidney cell proliferation and cyst formation. J Biol Chem. 2006; 281:29181–29189. [PubMed: 16870608]
29. O'Brien LE, Jou TS, Pollack AL, Zhang Q, Hansen SH, Yurchenco P, et al. Rac1 orientates epithelial apical polarity through effects on basolateral laminin assembly. Nat Cell Biol. 2001; 3:831–838. [PubMed: 11533663]
30. Bell PD, Fitzgibbon W, Sas K, Stenbit AE, Amira M, Houston A, et al. Loss of primary cilia upregulates renal hypertrophic signaling and promotes cystogenesis. J Am Soc Nephrol. 2011; 22:839–848. [PubMed: 21493775]
31. Besschetnova TY, Kolpakova-Hart E, Guan Y, Zhou J, Olsen BR, Shah JV. Identification of signaling pathways regulating primary cilium length and flow-mediated adaptation. Curr Biol. 2010; 26:182–187. [PubMed: 20096584]
32. Gray RS, Cheung KJ, Ewald AJ. Cellular mechanisms regulating epithelial morphogenesis and cancer invasion. Curr Opin Cell Biol. 2010; 22:640–650. [PubMed: 20832275]
33. Lu W, Peissel B, Babakhanlou H, Pavlova A, Geng L, Fan X, et al. Perinatal lethality with kidney and pancreas defects in mice with a targeted Pkd1 mutation. Nat Genet. 1997; 17:179–781. [PubMed: 9326937]
34. Zhou J. Polycystins and primary cilia: primers for cell cycle progression. Annu Rev Physiol. 2009; 71:83–113. [PubMed: 19572811]
35. Kim H, Bae Y, Jeong W, Ahn C, Kang S. Depletion of PKD1 by an antisense oligodeoxynucleotide induces premature G1/S-phase transition. Eur J Hum Genet. 2004; 12:433–440. [PubMed: 15054393]
36. Altman GH, Diaz F, Jakuba C, Calabro T, Horan RL, Chen J, et al. Silk-based biomaterials. Biomaterials. 2003; 24:401–416. [PubMed: 12423595]
37. Murphy AR, St John P, Kaplan DL. Modification of silk fibroin using diazonium coupling chemistry and the effects on hMSC proliferation and differentiation. Biomaterials. 2008; 29:2829–2838. [PubMed: 18417206]

38. Hines DJ, Kaplan DL. Mechanisms of controlled release from silk fibroin films. Biomacromolecules. 2011; 12:804–812. [PubMed: 21250666]
39. Shannon MB, Patton BL, Harvey SJ, Miner JH. A hypomorphic mutation in the mouse laminin alpha5 gene causes polycystic kidney disease. J Am Soc Nephrol. 2006; 17:1913–1922. [PubMed: 16790509]
40. Henry MD, Satz JS, Brakebusch C, Costell M, Gustafsson E, Fässler R, et al. Distinct roles for dystroglycan, beta1 integrin and perlecan in cell surface laminin organization. J Cell Sci. 2001; 114:1137–1144. [PubMed: 11228157]
41. Zhang X, Mernaugh G, Yang DH, Gewin L, Srichai MB, Harris RC, et al. beta1 integrin is necessary for ureteric bud branching morphogenesis and maintenance of collecting duct structural integrity. Development. 2009; 136:3357–3366. [PubMed: 19710172]
42. Wilson PD, Hrenuik D, Gabow PA. Abnormal extracellular matrix and excessive growth of human adult polycystic kidney disease epithelia. J Cell Physiol. 1992; 150:360–369. [PubMed: 1734038]
43. Qin S, Taglienti M, Nauli SM, Contrino L, Takakura A, Zhou J, et al. Failure to ubiquitinate c-Met leads to hyperactivation of mTOR signaling in a mouse model of autosomal dominant polycystic kidney disease. J Clin Invest. 2010; 120:3617–3628. [PubMed: 20852388]
44. Yu W, Datta A, Leroy P, O'Brien LE, Mak G, Jou TS, et al. Beta1-integrin orients epithelial polarity via Rac1 and laminin. Mol Biol Cell. 2005; 16:433–445. [PubMed: 15574881]
45. Streets AJ, Wagner BE, Harris PC, Ward CJ, Ong AC. Homophilic and heterophilic polycystin 1 interactions regulate E-cadherin recruitment and junction assembly in MDCK cells. J Cell Sci. 2009; 122(Pt 9):1410–1417. [PubMed: 19351715]
46. Perez VA, Ali Z, Alastalo TP, Ikeno F, Sawada H, Lai YJ, et al. BMP promotes motility and represses growth of smooth muscle cells by activation of tandem Wnt pathways. J Cell Biol. 2011; 192:171–188. [PubMed: 21220513]
47. Wilson PD, Geng L, Li X, Burrow CR. The PKD1 gene product, "polycystin-1," is a tyrosine-phosphorylated protein that colocalizes with alpha2beta1-integrin in focal clusters in adherent renal epithelia. Lab Invest. 1999; 79:1311–1323. [PubMed: 10532593]
48. Piontek K, Menezes LF, Garcia-Gonzalez MA, Huso DL, Germino GG. A critical developmental switc.h defines the kinetics of kidney cyst formation after loss of Pkd1. Nat Med. 2007; 13:1490–1495. [PubMed: 17965720]
49. Takakura A, Contrino L, Zhou X, Bonventre JV, Sun Y, Humphreys BD, et al. Renal injury is a third hit promoting rapid development of adult polycystic kidney disease. Hum Mol Genet. 2009; 18:2523–2531. [PubMed: 19342421]
50. Li X, Luo Y, Starremans PG, McNamara CA, Pei Y, Zhou J. Polycystin-1 and polycystin-2 regulate the cell cycle through the helix-loop-helix inhibitor Id2. Nat. Cell. Biol. 2005; 7:1202–1212. [PubMed: 16311606]

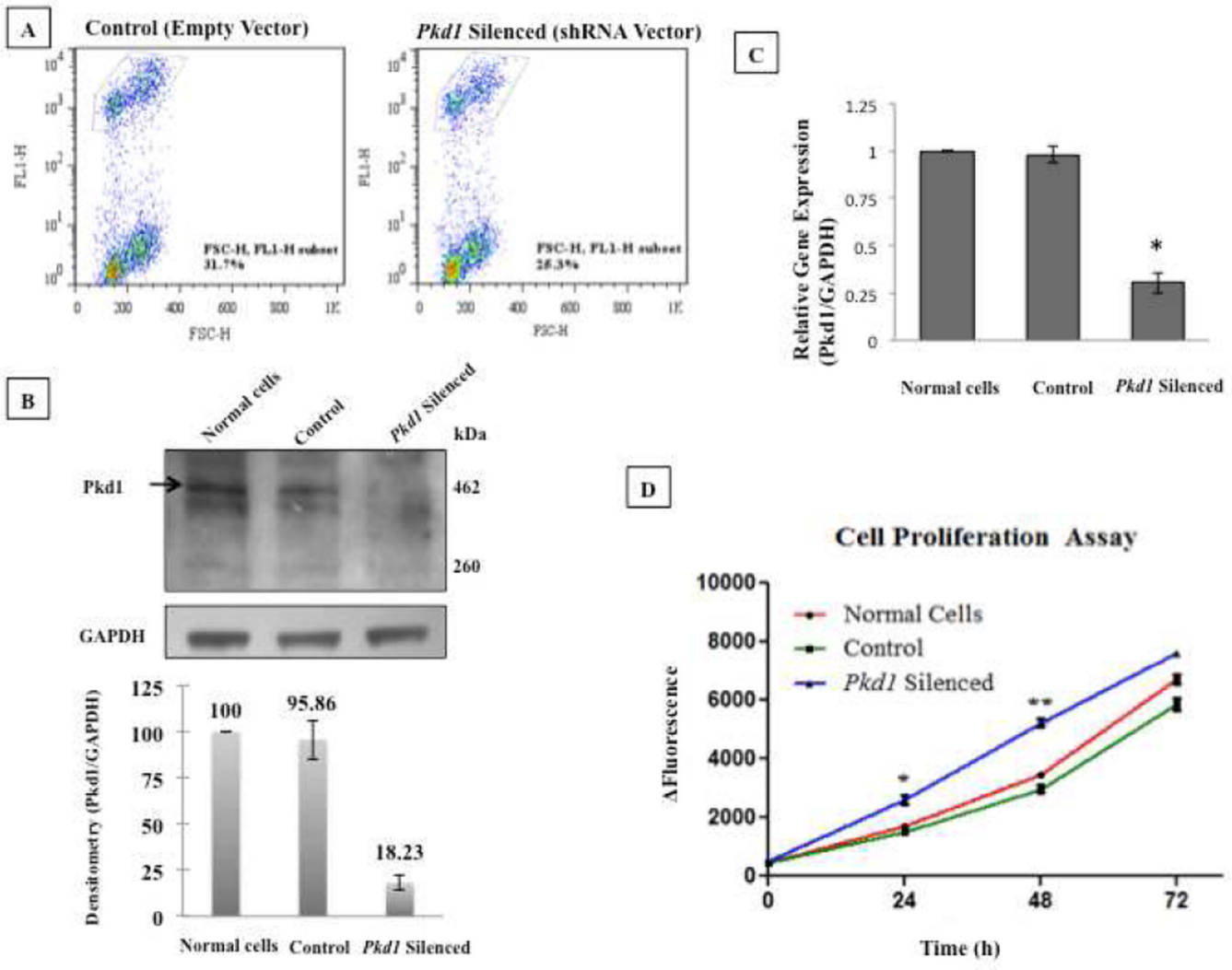

Figure 1. Generation and characterization of *Pkd1* knock down cells

(A) Flow cytometry analysis of lentivirus transduction. Cells were infected with a MOI-10 and evaluated in flow cytometry using GFP. Control vector infected cells showed 31.7% efficiency, while shRNA vector showed 25.3% efficiency. **(B) Knockdown analysis for *Pkd1*.** Total cell lysates were collected from the normal and transduced cells and blotted for Pkd1. Membrane was then stripped and probed for GAPDH to evaluate sample loading. At least three immunoblots from three independent lysate preparations was blotted for polycystin-1 and a representative blot was shown. The expression analysis of the Pkd1 relative to GAPDH was depicted in the bar graph below the immunoblot. Pkd1 expression was reduced by ~85% in shRNA transduced cells, while the expression level was not affected in control vector transduced cells. **(C) mRNA expression analysis of knockdown efficiency.** mRNA expression level of Pkd1 was determined in Control and *Pkd1* Silenced cells, normalized with respect to their GAPDH levels and compared with normal cells. *Pkd1* Silenced cells showed ~ 70% reduction in mRNA levels while minimal change was seen in Control cells. Statistical significance was seen *Pkd1* Silenced cells and other groups. (*p<0.01) **(D) Proliferation analysis in *Pkd1* Silenced cells.** Equal number of cells were plated and incubated with Alamar-blue dye at the specified times. Change in fluorescence was measured. Values were presented as mean ± SD. Statistical significance was seen

between *Pkd1* silenced cells and other group within 24h (*$p<0.05$) and increased at 48h (**$p<0.01$).

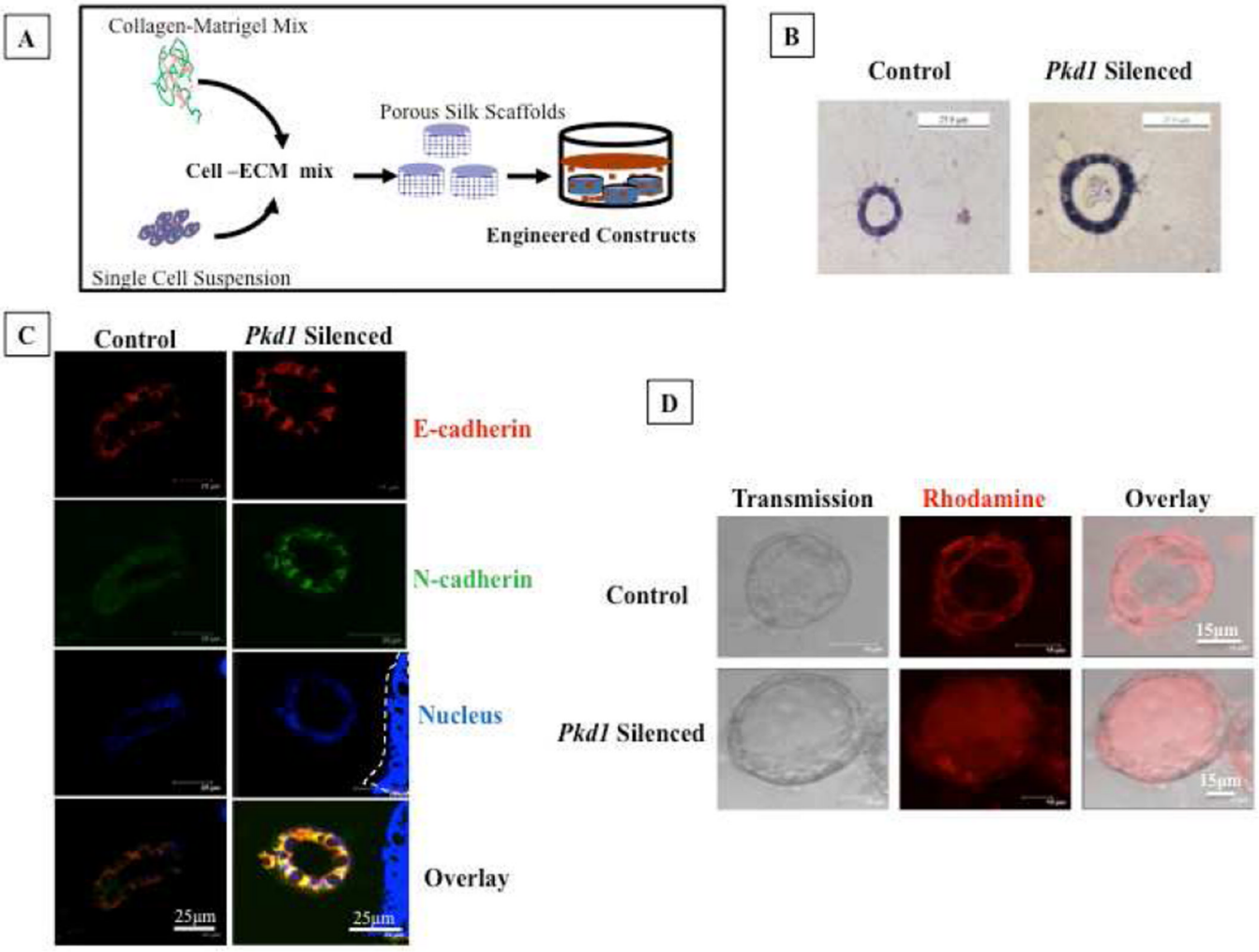

Figure 2. Engineered ADPKD cystic tissue model

(A) Schematic representation of stepwise procedure for developing cystic tissues in scaffolds. (B) H&E section of cystic structures developed at day 5 in control and Pkd1 Silenced cells. (C) Evaluation of structure using marker proteins. Immunofluorescence of cells stained for E-cadherin (red), N-cadherin (green) and nucleus (blue). Control cells exhibited membrane distribution for E-cadherin and minimal cytoplasmic expression for N-cadherin. *Pkd1* silenced cells exhibited membrane distribution for both the E-cadherin and N-cadherin. Scale bar 25μm. **(D) Evaluation of function using organic anion transport.** Whole scaffold live cell imaging for rhodamine in cystic structures in scaffolds. Control cells showed minimal uptake, while *Pkd1* silenced cells showed increased uptake and luminal secretion. Representative cyst images of normal and *Pkd1* Silenced cells were shown. Scale bar 15 μm.

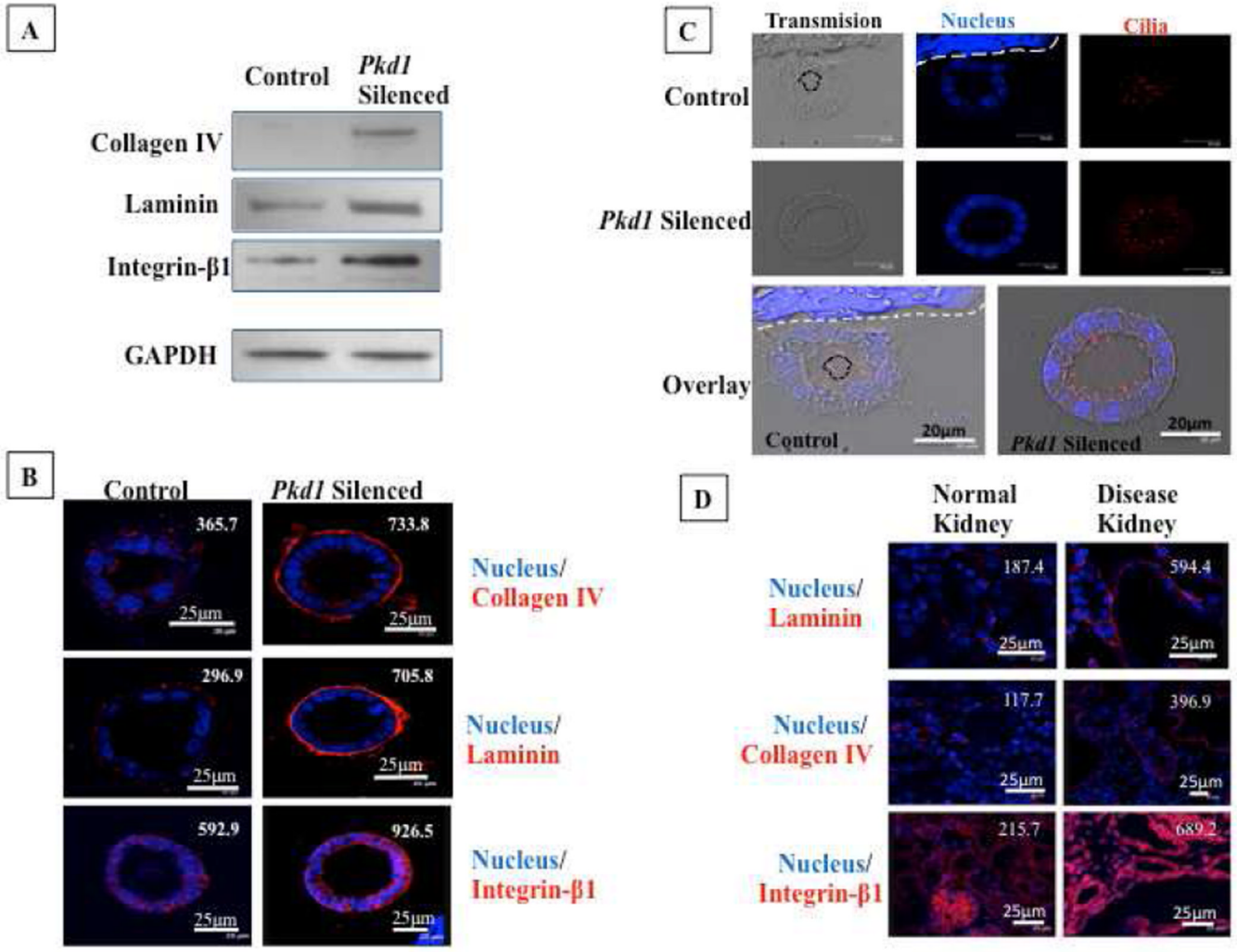

Figure 3. Abnormal matrix interactions in ADPKD cystic tissue model

(A) Evaluation of expression levels for matrix proteins (collagen-IV and laminin) and its receptor subunit protein, integrin-β1 in cell lysates. Total cell lysates collected from the cells grown on tissue culture treated plates were immunoblotted for collagen-IV, laminin and Integrin-β1. GAPDH levels were measured to evaluate the loading controls. *Pkd1* silenced cells showed an increased expression level of these proteins than control cells. **(B) Analysis of matrix proteins (collagen-IV and laminin) and its receptor subunit protein, integrin-β1, in tissue sections.** Numerical values included in upper right area of the images represent the fluorescence intensity per area units. Increased expression trend similar to the total lysates were observed in cysts developed from *Pkd1* silenced cells than control cells. Scale bar 25 μm. **(C) Evaluation of cilia in cystic structures.** Immunofluorescence of acetylated α-tubulin showed the existence of cilia in cystic structures developed from both control and *Pkd1* silenced cells. Scale bar 20 μm **(D) Analysis of matrix proteins (collagen-IV and laminin) and integrin-β1 in mouse kidney sections from normal and cystic (*Pkd1*$^{-/-}$) kidneys.** *Pkd1*$^{-/-}$ kidney sections exhibited increased expression than control kidney sections. Scale bar 25μm.

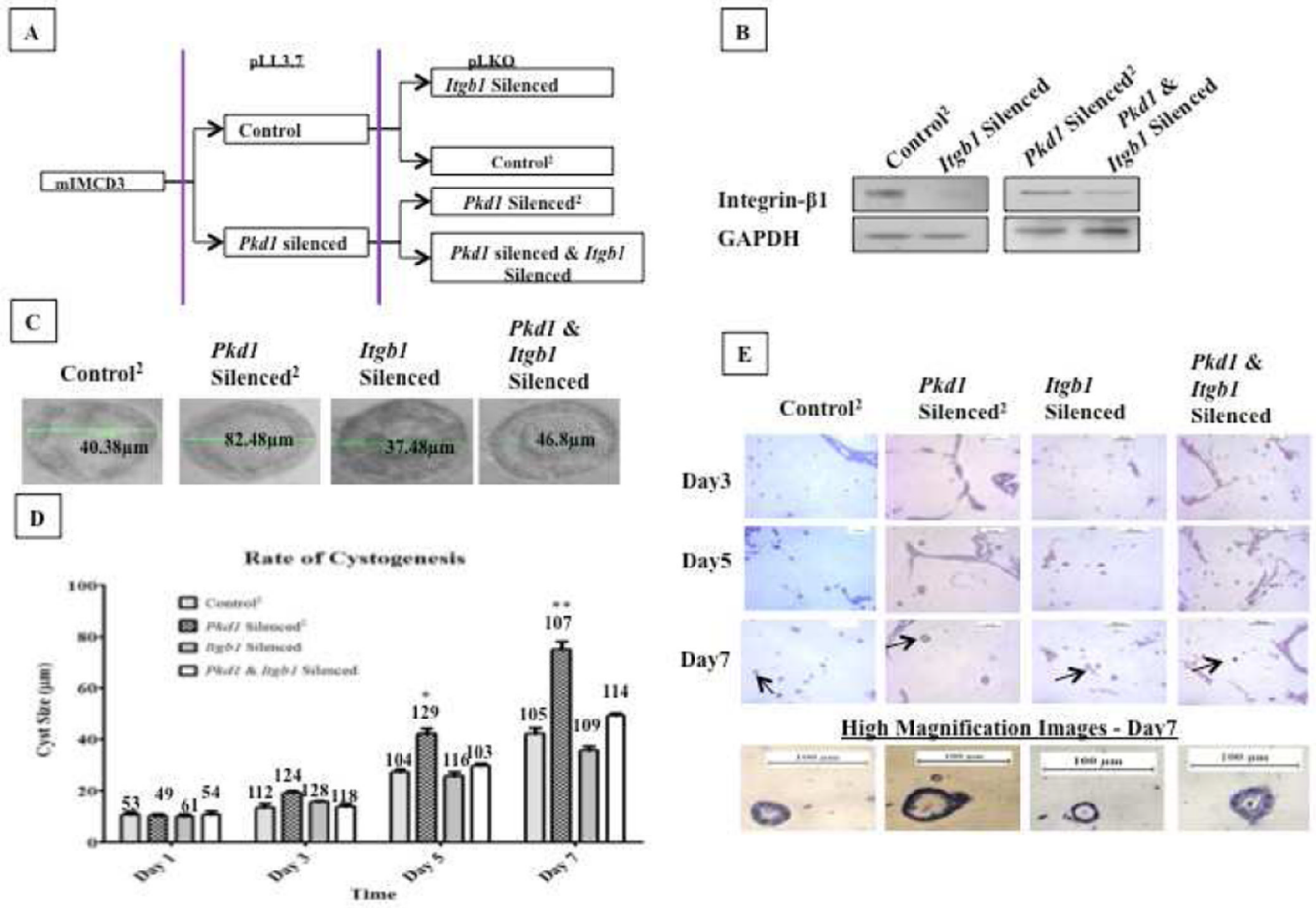

Figure 4. Abnormal matrix interactions regulate the rate of cystogenesis

(A) Schematic representation for the development of double silenced cells with their designated symbols. (B) Knockdown of Integrin-β1. Total cell lysates from double infected cells were immunoblotted for integrin-β1 and GAPDH. *Itgb1* silenced cells showed more than 90% decrease in protein than control vector infected cells (Control^2 cells). Similarly, *Pkd1* & *Itgb1* silenced cells showed 76% decrease than *Pkd1* silenced^2 cells. **(C–E) Evaluation of rate of cystogenesis.** Cells were serum starved for 72 h and plated as single suspension for 3D culture. Cyst images were collected at specified time points in transmission mode and their sizes were measured using the quantification tool in Leica Confocal Software. (C) Representative Day-7 cyst images developed in different cell lines. Quantification measurement is shown in green and its corresponding value is included in the image. (D) Rate of cyst formation over time. Size of the cysts observed at different time points in different cell lines were plotted as mean ± SD. Number of cyst scored for analysis were provided above their respective bars in the graph. *Pkd1* silenced^2 cells showed increased rate of cystogenesis than control^2 cells and is reversed in *Pkd1* & *Itgb1* silenced cells. In addition, *Itgb1* silenced cells showed minimal change in the rate of cystogenesis from control^2 cells. Statistical significance was seen at Day 5 (*$p<0.01$) and Day 7 (*$p<0.0001$) between Pkd1Silenced cells^2 and other cell lines. (E) Representative H&E section of cystic structures developed at different time points. Images were collected at 10X magnification. Cystic Structures were highlighted in Day 7 images. A similar trend of larger cyst structures were observed in *Pkd1* silenced^2 cells than other groups in Day 5 and Day 7. Lower panel represents a high magnification (40X) image of a cystic structures observed in different cell lines at Day 7. Scale bar 100 µm.

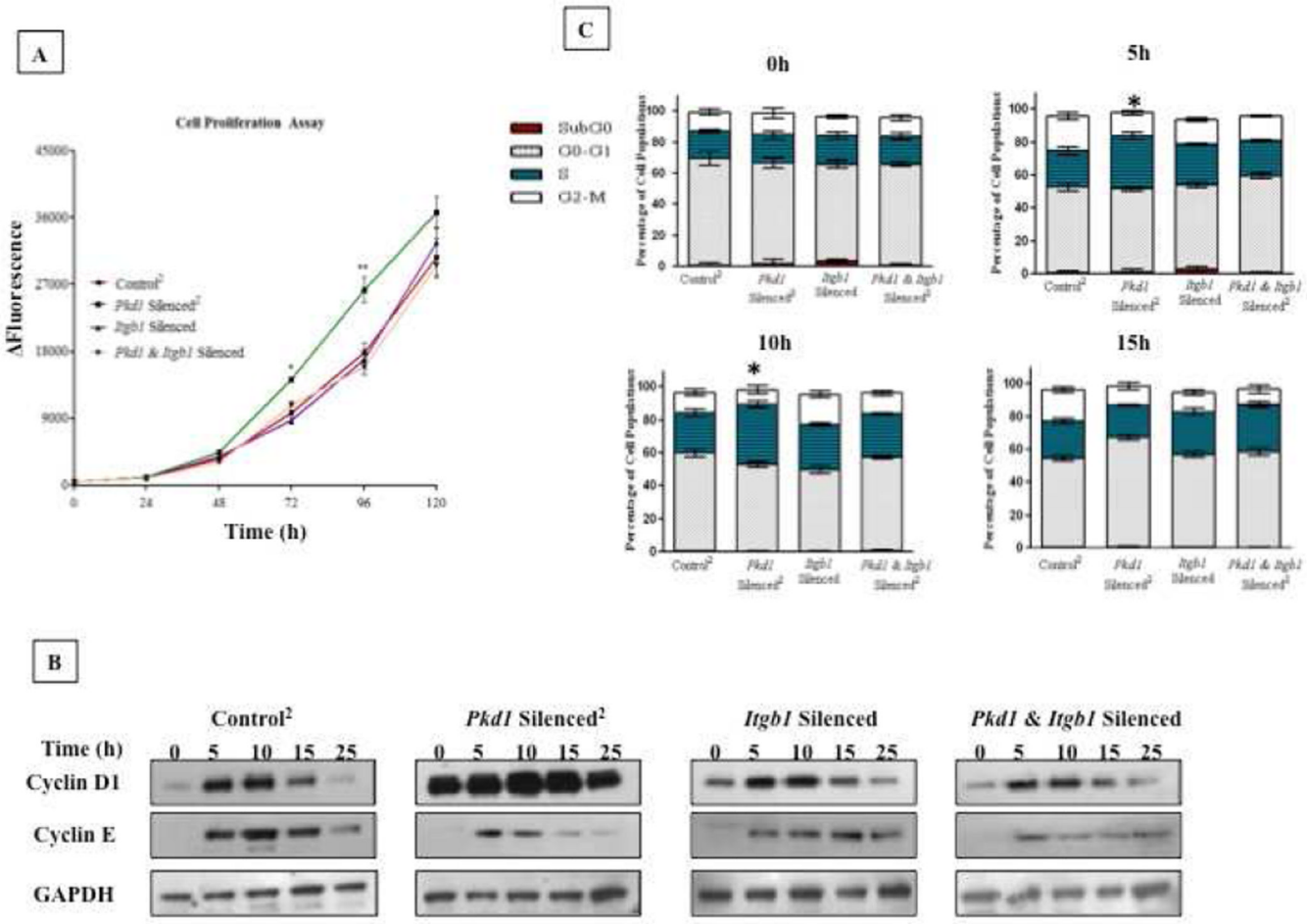

Figure 5. Proliferation and cell cycle changes are associated with the increased rate of cystogenesis

(A) Proliferation analysis in different cell lines. Equal number of cells were plated and incubated with Alamar dye at the specified time points. Change in fluorescence was measured and plotted with the time. *Pkd1* silenced^2 cells showed increased proliferation rate and is reversed in *Pkd1* & *Itgb1* silenced cells, similar to the rate of Control^2 and *Itgb1* silenced cells. **(B&C) Cell cycle analysis**. Cells were serum starved for 72 h and switched to regular media. Samples were collected at the specified time points. (B) Changes in cell cycle proteins, Cyclin- D1 and Cyclin-E, were measured over a time span of 25 h with specific time points. *Pkd1* silenced^2 cells showed constitutive up-regulation for Cyclin-D1, while other cell lines showed a profile similar to control^2 cells with a peak level at 10 h. For Cyclin-E, Control^2 and *Itgb1* silenced cells showed a similar profile with a 10–15 h peak level. *Pkd1* silenced^2 cells showed a peak level at 5 h. and are reversed significantly in *Pkd1* & *Itgb1* silenced cells. (C) Cells were harvested at specified time points and processed for DNA analysis in flow cytometry. Distribution of cells in different cell cycle phases were depicted as histograms in the graph and cell populations in S-phase was subjected to statistical analysis. *Pkd1* silenced^2 cells showed a significant increase in the number of cells in S-phase at 5 h and 10 h (*$p<0.05$) than other groups, while other cell populations showed a similar distribution profile. Values are represented as mean ± SD derived from three different set of experiments.

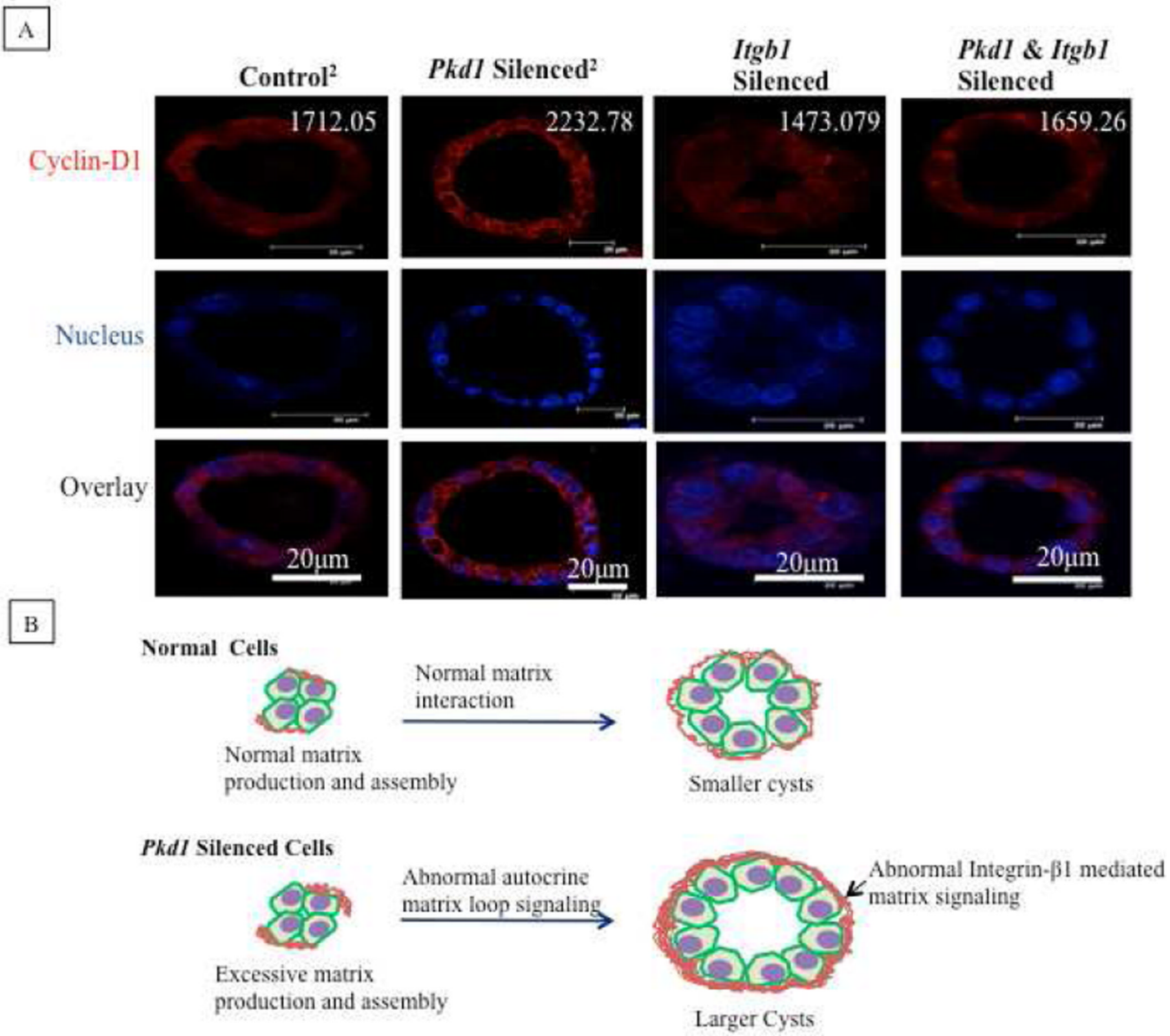

Figure 6.

(A) Cyclin-D1 exhibits increased expression in engineered cystic ADPKD tissue model. Parraffin sections of cystic structures were immunostained for Cyclin-D1. *Pkd1* Silenced[2] cells grown cysts showed increased expression and is reversed to normal conditions in *Pkd1* & *Itgb1* silenced cells grown cysts. Numerical value in each image represents the fluorescence intensity per area units. **(B) Summary-Model.** Loss of PKD1 function induces abnormal matrix deposition (collagen-IV and laminin) and its interacting receptor subunit protein (Integrin-β1). Abnormal matrix deposition acts reciprocally back on the cells through integrin-β1, alters cell cycle and proliferation, resulting in increased rate of cystogenesis. Disruption of this autocrine signaling in *Pkd1* silenced cells by double-silencing *Itgb1* renders the *Pkd1* silenced cells to reverse the cystogenesis rate to normal conditions.